Models for Image Interpolation based on the Optical Flow

Walter Hinterberger[†] and Otmar Scherzer[‡]

[†] *Industrial Mathematics Institute, University of Linz,*
Altenberger Str. 69, A-4040 Linz, Austria
E-Mail: `hinterberger@indmath.uni-linz.ac.at`
Web Page: `http://imagewww.indmath.uni-linz.ac.at`
[‡] *Department of Mathematics, Ludwig-Maximilian-University Munich*
Theresienstr. 39, 80333 München, Germany
E-Mail: `scherzer@rz.mathematik.uni-muenchen.de`

Optical flow is the 2D motion that needs to be recovered from a video sequence. In this paper we study variational principles for the generation of interpolating sequences between two images. The basic assumption is that there exists an underlying video sequence that solves the optic flow equation and interpolates the two images. The numerical solution of the interpolation problem is reduced to the solution of a system of coupled partial differential equations. Some numerical simulations are presented.

Key Words: Optical flow, image interpolation

1. INTRODUCTION

Optical flow is the 2D motion that needs to be recovered from a video sequence. 2D motions finds diverse applications in *video processing* and *compression* as well as in *computer vision*. In video compression the knowledge of motion helps to remove temporal data redundancy which in turn is used to compress video sequences with high compression rates. Motion estimation became a basic component of video compression standards, like e.g. MPEG. In video processing motion information is used for noise depression [7] and motion compensated restoration (deblurring) [18].

To compute motion trajectories, three basic elements need to be specified. First underlying models must be selected, like the motion model, the data relationship model and the occlusion model. There exist several excellent articles on the relationship between 3D motion and apparent 2D motions; we refer to [1, 12, 13, 17].

Image interpolation is the generation of a video sequence connecting two images (which will be referred to the initial and the final image in the course of this paper). Interpolation is relevant if the image acquisition is slow or expensive. In order to produce visually attractive interpolating video sequences appropriate motion models have to be specified. An easy and cheap possibility for interpolation is *blending* where the intensity of the initial image is linearly lowered while simultaneously the intensity of the final image is linearly increased; this procedure produces visually undesirable artifacts in the interpolating images. In this paper we consider sophisticated models for image interpolation based on appropriate motion models.

The outline of this paper is the following: in section 2 we outline the optical flow model. Later this serves as a starting point for image interpolation. The general ideas for the numerical calculation of motion fields are discussed in section 3. In sections 4, 5 we derive variational models for image interpolation based on the optical flow models. Naive implementations of optical flow results in undesirable artifacts in the interpolating sequence (cf. section 4). More sophisticated variational methods produce visually attractive interpolation sequences (cf. section 5). The numerical realization of such variational problems involves the solution of systems of coupled time dependent partial differential equations (cf. section 6). Some numerical experiments are presented.

2. MODELS FOR MOTION REPRESENTATION

Consider a point $\mathbf{X} = \mathbf{X}(t) = (X_1(t), X_2(t), X_3(t))^t$ on an object moving in an 3-dimensional space. $(\mathbf{X}(t), t)$ defines a curve in $\mathbb{R}^4$ which is usually called the *motion trajectory*. An image acquisition system projects the 3D world onto a 2D image plane with image coordinates $\mathbf{x} = \mathbf{x}(t) = (x_1(t), x_2(t))^t$. Upon this projection, the motion trajectory is projected on a 2-dimensional motion trajectory. The basics of every image motion estimation algorithm are assumptions about the relationship between motion parameters and image intensity. Typically one differs between two classes of models for motion representation.

- Since 2D motion results from a projection of moving 3D objects on a 2D image plane, the 2D motion is parametric if the 3D motion is parametric. Examples of parametric models are *affine linear* transformations,

$$\mathbf{X} \to A\mathbf{X} + b\,,$$

where $A \in \mathbb{R}^{3\times 3}$ and $b \in \mathbb{R}^3$. These models describe *global* displacements. The registered 2D motion is given as

$$\mathbf{X} \to \mathbf{x} = PA\mathbf{X} + Pb\,,$$

where P denotes the projector onto the acquisition plane.

- A different description of motion fields can be provided by 2D motion fields. In this way the number of parameters varies with the number of moving regions considered. In the extreme case the regions of uncorrelated movement are the pixels (*local* models).

In this paper we focus on local motion models. Let $I(\mathbf{x}, t)$ be the registered image intensity at position $(\mathbf{x}, t)$, with $\mathbf{x}$ in a reference domain Ω. A reasonable assumption is that the image intensity remains constant along the motion trajectory. This assumption implies that any intensity change is due to motion. Let $\mathbf{x}(t)$ be the parametrisation of a path of constant image intensity, i.e., $I(\mathbf{x}(t), t) = \textit{constant}$ for $t \in [0, \infty]$, then

$$\frac{\partial I}{\partial t}(\mathbf{x}(t), t) = 0\ . \tag{1}$$

By applying the chain rule, (1) can be written as the *motion constraint* (or *optical flow*) equation

$$\begin{aligned} 0 &= I_{x_1}(\mathbf{x},t)u(\mathbf{x},t) + I_{x_2}(\mathbf{x},t)v(\mathbf{x},t) + I_t(\mathbf{x},t) \\ &= (\nabla I)^t(\mathbf{x},t)\mathbf{w}(\mathbf{x},t) + I_t(\mathbf{x},t)\,, \end{aligned} \tag{2}$$

where $\mathbf{w}(\mathbf{x},t) = (u,v)^t(\mathbf{x},t)$.

In this paper we use the convention that subscripts denote partial derivatives and $\frac{\partial \cdot}{\partial t}$ denotes the *total* derivative. Moreover, for a function $f(x_1,x_2,t)$ defined on $\Omega \times [0,\infty)$ we use the following convention

$$\nabla f(\mathbf{x},t) = \left(f_{x_1}, f_{x_2}\right)^t(\mathbf{x},t) \text{ and } \nabla_t f(\mathbf{x},t) = \left(f_{x_1}, f_{x_2}, f_t\right)^t(\mathbf{x},t)\ .$$

Speaking with the words of continuum mechanics (for this topic we refer to [11]), the motion constraint equation is the Eulerian formulation of (1) in Lagrangian coordinates. Lagrangian formulations require a temporarily varying coordinate system.

The classical application of optical flow is to calculate the motion field between two images I^{init} and I^{end}. In this situation (2) can be considered at a stationary point, say 0. Therefore we can skip in (2) the time dependency and obtain

$$0 = (\nabla I)^t(\mathbf{x})\mathbf{w}(\mathbf{x}) + I_t(\mathbf{x})\ . \tag{3}$$

Usually, an approximation of $I_t(\mathbf{x})$ is provided by the finite difference approximation, $I^{\text{end}}(\mathbf{x}) - I^{\text{init}}(\mathbf{x})$. Approximations for $\nabla I(\mathbf{x})$ are typically obtained from finite difference approximations or by differentiating finite element approximations of convex combinations of the initial and the final image.

Assuming the initial condition $I^{\text{init}}(\mathbf{x}) = I(\mathbf{x},0)$, the approximation $I_t(\mathbf{x}) \sim I^{\text{end}}(\mathbf{x}) - I^{\text{init}}(\mathbf{x})$ implies that $I^{\text{end}}(\mathbf{x}) \sim I(\mathbf{x},1)$. As well as this particular choice, any approximation $I_t(\mathbf{x}) \sim \frac{I^{\text{end}}(\mathbf{x}) - I^{\text{init}}(\mathbf{x})}{h}$ is possible which asserts that $I(\mathbf{x},h)$ is an approximation for $Ie(\mathbf{x})$. The later choice leads to a scaled motion field (by a factor $1/h$).

The motion field is not determined by (3), since it is one equation for two unknown functions. Thus additional constraints have to imposed, and there are several models proposed in the literature. Optical flow simulations started with the pioneering work of Horn and Schunck [10] who proposed to calculate an approximate solution of (3) that minimizes the functional

$$J_{\text{HS}}(\mathbf{w}) = \frac{1}{2}\int_\Omega (|\nabla u(\mathbf{x})|^2 + |\nabla v(\mathbf{x})|^2)\, d\mathbf{x}\ . \tag{4}$$

Recently there has been a trend to use more sophisticated constraints to enhance edges and corners in the motion field (see e.g. [15, 4, 19, 21]). This can be achieved by considering penalizing functionals of the form

$$J_{\text{NE}}(\mathbf{w}) = \int_\Omega \text{trace}\Big((\nabla \mathbf{w}(\mathbf{x}))^t D_2(\nabla I)(\mathbf{x})(\nabla \mathbf{w}(\mathbf{x}))\Big)\,,$$

with

$$D_2(\nabla I)(\mathbf{x}) = \frac{1}{\|\nabla I(\mathbf{x})\|^2 + 2\lambda^2}\left\{ \begin{pmatrix} \frac{\partial I}{\partial x_2}(\mathbf{x}) \\ -\frac{\partial I}{\partial x_1}(\mathbf{x}) \end{pmatrix} \begin{pmatrix} \frac{\partial I}{\partial x_2}(\mathbf{x}) \\ -\frac{\partial I}{\partial x_1}(\mathbf{x}) \end{pmatrix}^t + \lambda^2 I \right\}\ .$$

Here and in the sequel of the paper $||.||$ denotes the Euclidean norm and I denotes the unitary matrix. The motivation for using such penalizing functionals comes from anisotropic diffusion filtering. For some background on this topic we refer to [2, 3, 8, 22]. Nonlinear penalizing functionals with temporal dependency for the solution of optical flow problems have been studied by Schnörr and Weickert [19].

Following the standard way of solving a constraint optimization problem, an approximate minimizers of J_{HS} that solves (3) is obtained by solving the *unconstraint* optimization problem, to minimize the functional

$$J_{\text{HS}}^{\lambda}(\mathbf{w}) = \lambda \int_{\Omega} ((\nabla I)^t \mathbf{w} + I_t)^2(\mathbf{x}) + J_{\text{HS}}(\mathbf{w}) \,, \tag{5}$$

where λ is the positive *Lagrange* (or *penalizing*) parameter.

3. NUMERICAL SOLUTION OF THE OPTICAL FLOW EQUATION

In this section we outline a numerical procedure to solve optic flow problems. For the sake of simplicity of presentation we restrict our attention to the calculation of the solution of the motion constraint equation (3) that minimizes the functional J_{HS}. The use of other constraints is conceptionally rather similar [21, 19]. Formal differentiation of the functional J_{HS}^{λ} with respect to $\mathbf{w} = (u, v)^t$ shows that the minimizer satisfies the system of partial differential equations

$$\begin{aligned} \Delta u(\mathbf{x}) - 2\lambda I_{x_1}(\mathbf{x})\Big(I_{x_1}(\mathbf{x})u(\mathbf{x}) + I_{x_2}(\mathbf{x})v(\mathbf{x}) + I_t(\mathbf{x})\Big) &= 0 \,, \\ \Delta v(\mathbf{x}) - 2\lambda I_{x_2}(\mathbf{x})\Big(I_{x_1}(\mathbf{x})u(\mathbf{x}) + I_{x_2}(\mathbf{x})v(\mathbf{x}) + I_t(\mathbf{x})\Big) &= 0 \,, \end{aligned} \tag{6}$$

with homogeneous Neumann boundary conditions; here Δ denotes the Laplacian.

(6) can be thought as the steady-state of the reaction diffusion process

$$\begin{aligned} u_\theta(\mathbf{x},\theta) = \Delta u(\mathbf{x},\theta) - 2\lambda I_{x_1}(\mathbf{x})\Big(I_{x_1}(\mathbf{x})u(\mathbf{x},\theta) + I_{x_2}(\mathbf{x})v(\mathbf{x},\theta) + I_t(\mathbf{x})\Big) &= 0 \,, \\ v_\theta(\mathbf{x},\theta) = \Delta v(\mathbf{x},\theta) - 2\lambda I_{x_2}(\mathbf{x})\Big(I_{x_1}(\mathbf{x})u(\mathbf{x},\theta) + I_{x_2}(\mathbf{x})v(\mathbf{x},\theta) + I_t(\mathbf{x})\Big) &= 0 \,, \end{aligned} \tag{7}$$

where θ denotes an evolution parameter, which should not be confused with the time t in the motion constraint equation (3). The system (7) can be solved by a explicit or implicit scheme with respect to the evolution parameter and $\mathbf{w}(\mathbf{x}) = \mathbf{w}(\mathbf{x}, \infty)$ is the solution of (6) (see e.g. [21, 19]).

4. NAIVE APPROACH FOR IMAGE INTERPOLATION

The naive approach to image interpolation based on motion models is to displace every pixel into the direction of a local motion. The solution of (7) gives an evolution parameter dependent motion. The interpolating images can be calculated by displacing every pixel along the motion field. This approach leads to undesirable artifacts. The reason for the failure of this method is that it interpolates the motion field $\mathbf{w}$ and not the image intensity itself. Moreover, the motion constraint equation is not capable to detect the motion field appropriately if the two images I^{end} and I^{init} show large deviations (see e.g. [4]). One of the disastrous numerical experiment has been plotted in figure 1. For the local motion fields calculated from (7) motion trajectories cross or do not touch the final image and consequently shocks and holes form.

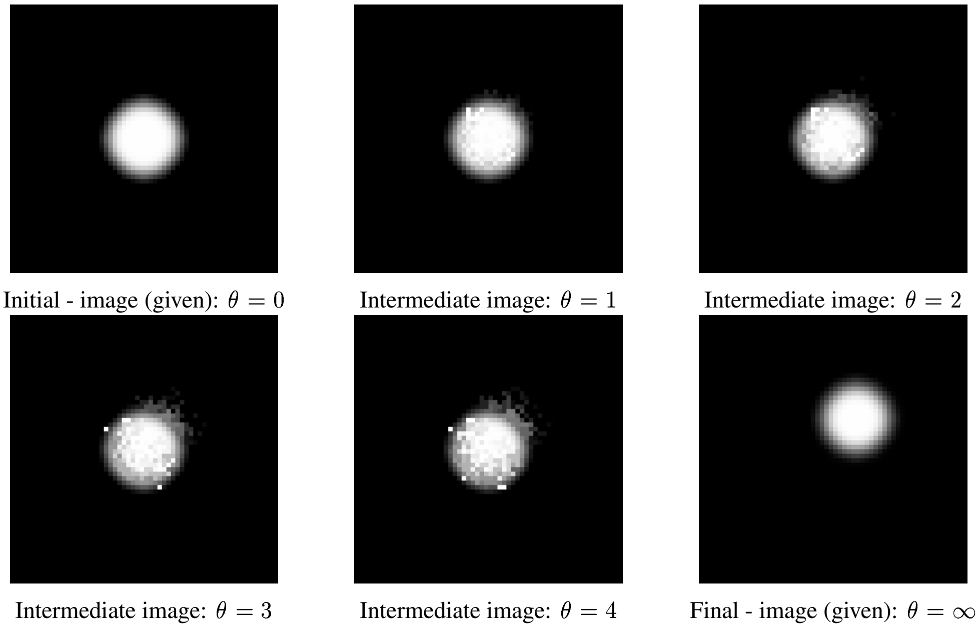

FIG. 1. Naive use of the optic flow for image interpolation!

5. MODELS FOR IMAGE INTERPOLATION

The optical flow equation (3) is capable to describes motion fields between two images with small displacements. A *non-local* algorithm has been proposed by Nagel and Enkelmann [14], to minimize the functional J_{NE} under the (least squares) solutions $\mathbf{w} = (u, v)^t$ of

$$I^{\text{end}}(\mathbf{x}) = I^{\text{init}}(x_1 + u(\mathbf{x}), x_2 + v(\mathbf{x})) \; . \tag{8}$$

A modification of this approach has been suggested by Alvarez, Weickert, and Sánchez [4]. Deformable templates models have been studied by Amit et. al. [5, 6], Thirion [20], Fischer and Modersitzki [9], to name but a few.

In the following we discuss a generalization of the Nagel and Enkelmann model. Let $\mathbf{w}(., t) = (u(., t), v(., t))^t$ be a smooth motion field and let I be a solution of (2) with initial data

$$I(\mathbf{x}, 0) = I^{\text{init}}(\mathbf{x}) \text{ for } \mathbf{x} \in \Omega \; . \tag{9}$$

Since we are not aware of any existence and uniqueness result for (2), (9), we consider *singularly* perturbed problems.

A *parabolic singular perturbed* problem of (2) is

$$I_t(\mathbf{x}, t) - \beta \nabla . (K_2(\nabla I)) + (\nabla I)^t(\mathbf{x}, t)\mathbf{w}(\mathbf{x}, t) = 0 \, ,$$

with homogeneous Dirichlet boundary conditions on $\partial\Omega$ and initial condition (9). Here β a small positive parameter and $-\nabla.(K_2(\nabla.))$ is a continuous, strongly elliptic differential operator on $H_0^1(\Omega)$ (the subspace of functions in the Sobolev space $H^1(\Omega)$ that vanish on $\partial\Omega$). The operator is strongly elliptic if there exists a positive constant ε such that

$$\int_\Omega K_2(\nabla\tilde{I})\nabla\tilde{I} \geq \varepsilon \int_\Omega \|\nabla\tilde{I}\|^2 ,$$

for any real valued function $\tilde{I} \in H_0^1(\Omega)$. Moreover, this operator is continuous, if for any two functions $\tilde{I}, \tilde{\tilde{I}} \in H_0^1(\Omega)$

$$\left|\int_\Omega K_2(\nabla\tilde{I})\nabla\tilde{\tilde{I}}\right| \leq c\sqrt{\int_\Omega \|\nabla\tilde{I}\|^2 \int_\Omega \|\nabla\tilde{\tilde{I}}\|^2} .$$

In this paper we consider singular perturbations with homogeneous Dirichlet boundary conditions on $\partial\Omega$. This assumption is reasonable if we consider images with *zero frame*. All along this paper we write "a solution of (2)" but actually mean a solution of a singular (parabolic) perturbed problem.

For the purpose of image interpolation we calculate simultaneously a time dependent motion field $\mathbf{w}$ and a solution $I := I(\mathbf{w})$ of (2), (9) that satisfy (at least in a least squares sense)

$$I^{\text{end}}(\mathbf{x}) = I(\mathbf{x}, 1) . \tag{10}$$

From the set of solutions we select one that minimizes one of the following penalizing functionals:

The (time dependent) Horn-Schunck functional:

$$J_{\text{HS}_t}(\mathbf{w}) = \frac{1}{2}\int_0^1 \int_\Omega \|\nabla\mathbf{w}(\mathbf{x}, t)\|^2 d\mathbf{x}\, dt .$$

This functional is defined on the space $\mathcal{D}(J_{\text{HS}_t}) = \left(L^2((0,1); H_0^1(\Omega))\right)^2$. For a definition of the *Bochner space* $L^2((0,1); H_0^1(\Omega))$ we refer to [23]; the $.^2$ in the definition of $\mathcal{D}(J)$ symbolizes the product of two Bochner spaces.

The H^1-seminorm on $\Omega \times (0,1)$

$$J_{H_t^1}(\mathbf{w}) = \int_0^1 \int_\Omega \|\nabla_t \mathbf{w}(\mathbf{x}, \tau)\|^2 \; d\mathbf{x}\, d\tau .$$

This functional is considered on the space

$$\mathcal{D}(J_{H_t^1}) = \{f \in H^1(\Omega \times (0,1)) : f(x,t) = 0 \text{ for } x \in \partial\Omega, t \in (0,1)\}^2 .$$

The averaged Nagel and Enkelmann functional: for $I := I(w)$, let

$$J_{\text{NE}_a}(\mathbf{w}) = \int_0^1 \int_\Omega \text{trace}\left((\nabla\mathbf{w}(\mathbf{x},\tau))^t \tilde{D}_2(\nabla I)(\mathbf{x},\tau)\nabla\mathbf{w}(\mathbf{x},\tau)\right) \; d\mathbf{x}\, d\tau , \tag{11}$$

with uniformly bounded and uniformly positive definite matrices $\tilde{D}_2(\nabla I)(\mathbf{x},\tau) \in \mathbb{R}^2_2$, i.e., for all $I := I(\mathbf{w})$ and all $(\mathbf{x},\tau) \in \Omega \times (0,1)$,

$$\begin{aligned} \mathbf{v}^t \tilde{D}_2(\nabla I)(\mathbf{x},\tau)\mathbf{v} &\geq \varepsilon \|\mathbf{v}\|^2 \quad \text{for all } \mathbf{v} \in \mathbb{R}^2 \\ \left|\mathbf{v}^t \tilde{D}_2(\nabla I)(\mathbf{x},\tau)\tilde{\mathbf{v}}\right| &\leq c\|\mathbf{v}\|\|\tilde{\mathbf{v}}\| \quad \text{for all } \mathbf{v}, \tilde{\mathbf{v}} \in \mathbb{R}^2 \ . \end{aligned}$$

The averaged Nagel and Enkelmann penalizing functional is considered on the space $\mathcal{D}(J_{\text{NE}_a}) = L^2((0,1); H^1_0(\Omega))^2$.

The time dependent Nagel and Enkelmann functional: for $I := I(\mathbf{w})$ let

$$J_{\text{NE}_t}(\mathbf{w}) = \int_0^1 \int_\Omega \text{trace}\left((\nabla_t \mathbf{w}(\mathbf{x},\tau))^t \tilde{D}_3(\nabla_t I)(\mathbf{x},\tau) \nabla_t \mathbf{w}(\mathbf{x},\tau) \right) \, d\mathbf{x}\, d\tau \ , \tag{12}$$

with uniformly bounded and uniformly positive definite matrices $\tilde{D}_3(\nabla_t I)(\mathbf{x},t) \in \mathbb{R}^3_3$. This functional is defined on

$$\mathcal{D}(J_{\text{NE}_t}) = \{ f \in H^1(\Omega \times (0,1)) : f(x,t) = 0 \text{ for } x \in \partial\Omega, t \in (0,1) \}^2 \ .$$

Let J be either one of the functionals described above and let $\mathcal{D}(J)$ be the associated set of admissible functions. The minimizers of the functional

$$E(\mathbf{w}) = \frac{\lambda}{2} \int_0^1 \|I(.,\tau) - I^{\text{end}}(.)\|^2_{L^2(\Omega)} \, d\tau + \frac{1}{2} J(\mathbf{w}) \tag{13}$$

approximate the solutions of the constraint optimization problem. In the functional $\lambda > 0$ is the Lagrange parameter and $I := I(\mathbf{w})$ is a solution of (2). For notational reason we avoid indication of the dependency $I := I(\mathbf{w})$ as long as there is no danger of confusion.

The optical flow model (3) is unsymmetric in the sense that interpolating sequences may be different when I^{end} is considered as initial image and I^{init} is considered as final image, i.e., the roles of I^{end} and I^{init} are interchanged. In the following we symmetric the functional E. Let $\hat{I}$ be the solution of

$$\hat{I}_t(\mathbf{x},t) + (\nabla \hat{I})^t(\mathbf{x},t)\mathbf{w}(\mathbf{x},t) = 0 \text{ with } \mathbf{x} \in \Omega \text{ and } t \in [0,1] \ . \tag{14}$$

with initial data

$$\hat{I}(\mathbf{x},0) = I^{\text{end}}(\mathbf{x}) \ . \tag{15}$$

For the calculation of two spatially and temporarily varying motion fields $\mathbf{w} = (u,v)^t$ and $\hat{\mathbf{w}} = (\hat{u},\hat{v})^t$ in $\Omega \times [0,1]$ that satisfy (at least in a least squares sense)

$$I(t) = \hat{I}(1-t) \ ,$$

the functional

$$E_s(\mathbf{w},\hat{\mathbf{w}}) := \frac{\lambda}{2} \int_0^1 \int_\Omega \left(I(\mathbf{w})(\mathbf{x},\tau) - \hat{I}(\hat{\mathbf{w}})(\mathbf{x},1-\tau) \right)^2 \, d\tau\, d\mathbf{x} + \frac{1}{2} J_2(\mathbf{w},\hat{\mathbf{w}}) \ , \tag{16}$$

has to be minimized. Here $J_2(\mathbf{w},\hat{\mathbf{w}}) = J(\mathbf{w}(.,t)) + J(\hat{\mathbf{w}})(1-t)$.

The motivation for using the first term in (13) is to attract I as fast as possible to the final states I^{end}. If we require that the solution is attracted to I^{end} (without requiring "as fast as possible") a suitable optimization functional is

$$E_1(w) = \frac{\lambda}{2}\|I(.,1) - I^{\text{end}}(.)\|^2_{L^2(\Omega)} + \frac{1}{2}J(\mathbf{w}) \; .$$

An analytical expression for the Gateaux derivative, which forms the basis of most minimization algorithms, is more difficult to derive for E_1 than for E. In the following section we derive the analytical expression of the Gateaux derivative of the functional E.

6. NUMERICAL REALIZATION AND DISCUSSION OF THE NUMERICAL EXPERIMENTS

Below we describe minimization of the functional E with $J = J_{HS_t}$. The procedure of minimizing E with other penalizing functionals than J_{HS_t} is analogous and thus omitted. The solution of (2) gives the interpolated sequence.

The standard procedure for calculating the minimizer of E is to solve the *Euler equation*

$$E'(\mathbf{w}) = 0 \,, \tag{17}$$

where E' is the Gateaux derivative of E. If E is convex, then the solutions of (17) are the minimizing elements of E and vice versa.

Let $E_h = E(\mathbf{w} + h\mathbf{r})$, with $h \in \mathbb{R}$ and $\mathbf{r} = (r_1, r_2)^t$, then

$$\begin{aligned}
&\frac{E_h - E}{h} \\
&= \frac{\lambda}{2}\lim_{h\to 0}\int_0^1\int_\Omega \frac{\|I(\mathbf{w}+h\mathbf{r}) - I^{\text{end}}\|^2 - \|I(\mathbf{w}) - I^{\text{end}}\|^2}{h} \\
&+ \lim_{h\to 0}\frac{1}{2}\int_0^1\int_\Omega \frac{\|\nabla(\mathbf{w}+h\mathbf{r})\|^2 - \|\nabla\mathbf{w}\|^2}{h} \\
&= \lambda\int_0^1\int_\Omega (I(\mathbf{w}) - I^{\text{end}})(I_u((r_1,0)^t) + I_v((0,r_2)^t) \\
&+ \int_0^1\int_\Omega \nabla\mathbf{w}\nabla\mathbf{r} \; .
\end{aligned}$$

Here $I_u((r_1,0)^t) := I_u(\mathbf{w})((r_1,0)^t)$, $I_v((0,r_2)^t) := I_v(\mathbf{w})((0,r_2)^t)$ denote the Gateaux-derivatives of $I(\mathbf{w})$ in the directions $(r_1,0)^t$ and $(0,r_2)^t$, respectively, i.e.,

$$I_u(r_1) = \lim_{h\to 0}\frac{I(u+hr_1,v) - I(u,v)}{h} \text{ and } I_v(r_2) = \lim_{h\to 0}\frac{I(u,v+hr_2) - I(u,v)}{h} \; .$$

Thus

$$E'(\mathbf{w})\mathbf{r} = \begin{pmatrix} \lambda\left(\frac{\partial I}{\partial u}\right)^*(\mathbf{w})\big(I(\mathbf{w}) - I^{\text{end}}\big)(\mathbf{x},t) - \Delta u(\mathbf{x},\tau) \\ \lambda\left(\frac{\partial I}{\partial v}\right)^*(\mathbf{w})\big(I(\mathbf{w}) - I^{\text{end}}\big)(\mathbf{x},t) - \Delta v(\mathbf{x},\tau) \end{pmatrix} \; .$$

Here $.^*$ denotes the adjoint operator with respect to the $L^2(\Omega)$–norm, i.e., for a continuous operator T the adjoint operator T^* satisfies

$$\int_\Omega T(u)v = \int_\Omega uT^*(v) \text{ for all } u,v \in L^2(\Omega) \; .$$

The Gateaux derivative of I in direction $\mathbf{r}$ is the vector valued operator

$$I_G(\mathbf{w})(\mathbf{r}) := (I_u, I_v) := \left(I_u(\mathbf{w})(r_1,0)^t, I_v(\mathbf{w})(0,r_2)^t\right) \ . \tag{18}$$

Formal calculations show that $I_u := I_u(\mathbf{w})$, $I_v := I_v(\mathbf{w})$ satisfy the system of coupled *inhomogeneous optical flow equations*

$$(I_u)_t + (I_u)_{x_1}u + (I_u)_{x_2}v = -I_{x_1}r_1 \text{ and } (I_v)_t + (I_v)_{x_1}u + (I_v)_{x_2}v = -I_{x_2}r_2 \ , \tag{19}$$

with initial data

$$I_u(\mathbf{x},0) = I_v(\mathbf{x},0) = 0 \ \text{ for } \mathbf{x} \in \Omega.$$

Again for singular perturbed equations there exist solutions.

Now, we derive the explicit representations for the operators I_u^* and I_v^*. For given motion field $\mathbf{w}$ let L be the solution of

$$L_t(\mathbf{x},t) + (L\cdot u)_{x_1}(\mathbf{x},t) + (L\cdot v)_{x_2}(\mathbf{x},t) = I(\mathbf{x},t) - I^{\text{end}}(\mathbf{x}) \tag{20}$$

satisfying the *final* data

$$L(\mathbf{x},1) = 0 \text{ for } \mathbf{x} \in \Omega \ . \tag{21}$$

As usual there exists a solution of a singular perturbed equation.

Formal integration by parts gives

$$\int_0^1 \int_\Omega (I - I^{\text{end}}) I_u((r_1,0)^t) = \int_0^1 \int_\Omega L I_{x_1}(\mathbf{w}) r_1 \ ,$$

which shows $I_u^* = LI_{x_1}, I_v^* = LI_{x_2}$. Thus the Euler equation can be rewritten as

$$0 = \lambda L I_{x_1}(\mathbf{w})(\mathbf{x},t) - \Delta u(\mathbf{x},t) \text{ and } 0 = \lambda L I_{x_2}(\mathbf{w})(\mathbf{x},t) - \Delta v(\mathbf{x},t) \ . \tag{22}$$

The coupled system of partial differential equation (20),(22), and (2) is extremely expensive to solve numerically, since it involves the differential equation (20), which is *backward* in time (20) and the differential equation (2), which is *forward* in time. I comparison to standard non–local image matching models (see e.g. [14, 5, 6, 4]) the model (20), (22) and (2) is more complicated due to the additional involvence of L.

To avoid extremely expensive calculations involving a system of differential equations backward and forward in time we approximate L by

$$\hat{L}(\mathbf{w})(\mathbf{x},t) = (t-1)\left(I(\mathbf{w})(\mathbf{x},t) - I^{\text{end}}(\mathbf{x})\right) \ .$$

This approximation shares common features with L: it satisfies the final condition (21). For $t \to 1$, $I(\mathbf{w})(.,t)$ approximates the stationary state I^{end}. Thus we have

$$I_t(.,t) + (\hat{L}u)_{x_1}(.,t) + (\hat{L}v)_{x_2}(.,t) \sim 0 \text{ for } t \text{ in a neighborhood of } 1 \ .$$

$\hat{L}$ does **not** approximate L in a *very small* neighborhood of 0. To see this, we define the function

$$f(t) := |t-1| \sqrt{\int_\Omega \left((I_t(\mathbf{x},t) + (I(\mathbf{w}) - I^{\text{end}})u)_{x_1}(\mathbf{x},t) + ((I(\mathbf{w}) - I^{\text{end}})v)_{x_2}(\mathbf{x},t)\right)^2 dx} \ .$$

If f vanishes then $\hat{L}$ is a solution of (20). For the numerical experiments represented in figure 5 we have plotted the associated function f in figure 3. The function f is only significantly different from 0 in a very small neighborhood of 0. Thus we might expect that $\hat{L}$ approximates L and thus in turn I_u^*.

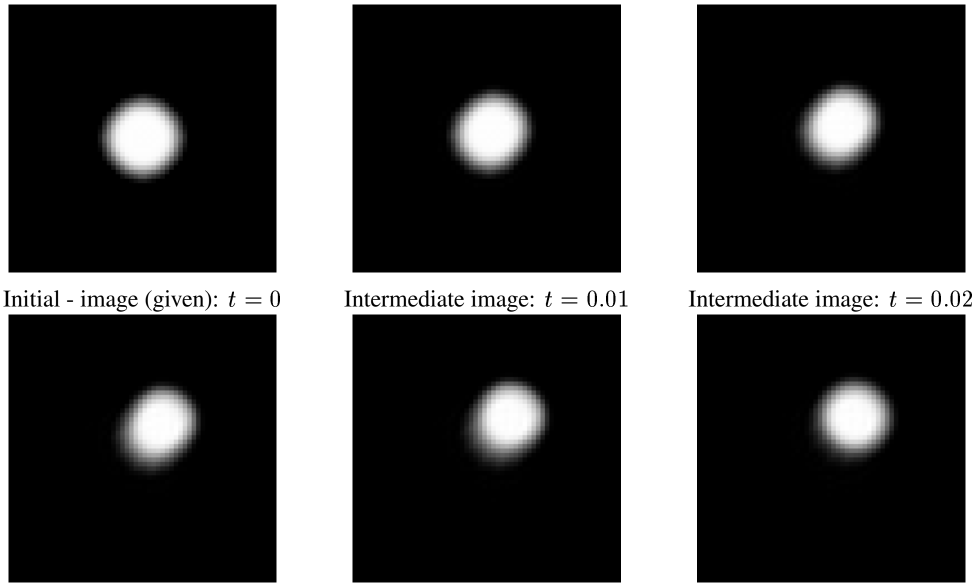

Initial - image (given): $t = 0$ Intermediate image: $t = 0.01$ Intermediate image: $t = 0.02$

Intermediate image: $t = 0.04$ Intermediate image: $t = 0.08$ Intermediate image: $t = 1$

FIG. 2. Interpolation between two displaced circles

In figure 2 the interpolating sequence is plotted at an exponentially increasing sequence of time instances. This gives the visually most attractive interpolating sequence; the functional (13) attracts the image sequence “as fast as possible” to the final image (this is achieved by integration of the first term in (13) with respect to the time variable). Thus one might expect large changes in the beginning and small changes near $t = 1$. Figure 4 shows blending, i.e., the intensity of the initial image is linearly lowered while the intensity of the final image is linearly increased. The interpolating sequence is visually more natural.

Replacing L by $\hat{L}$ in (22) leads us to a system of partial differential equations which is completely forward in time

$$\begin{aligned} 0 &= (t-1)\lambda I_{x_1}(\mathbf{w})\big(I(\mathbf{w}) - I^{\text{end}}\big)(\mathbf{x},t) - \Delta u(\mathbf{x},t) \\ 0 &= (t-1)\lambda I_{x_2}(\mathbf{w})\big(I(\mathbf{w}) - I^{\text{end}}\big)(\mathbf{x},t) - \Delta v(\mathbf{x},t) \\ 0 &= I_t + I_{x_1}u + I_{x_2}v\ . \end{aligned} \tag{23}$$

All numerical results where obtained by solving the system of partial differential equations (23).

Figure 2 shows the interpolating sequence between two displaced circles. In comparison with the naive approach in section 4 holes and shocks are prevented.

In figure 2 the interpolating sequence is plotted at an exponentially increasing sequence of time instances. This gives the visually most attractive interpolating sequence; the functional (13) attracts the image sequence “as fast as possible” to the final image (this is

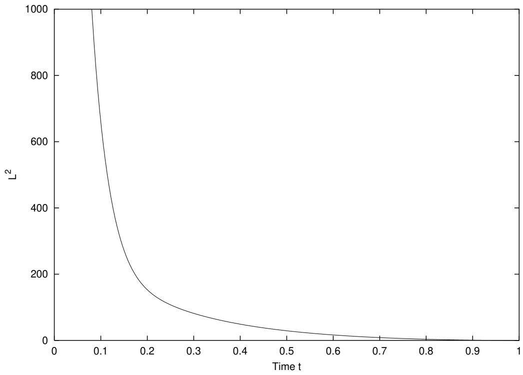

FIG. 3. Time plot of the function $f(t)$.

achieved by integration of the first term in (13) with respect to the time variable). Thus one might expect large changes in the beginning and small changes near $t = 1$. Figure 4 shows blending, i.e., the intensity of the initial image is linearly lowered while the intensity of the final image is linearly increased. The interpolating sequence is visually more natural.

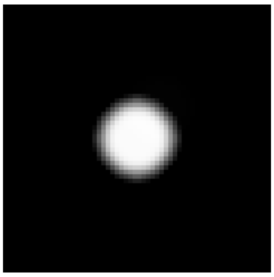
Initial - image (given): $t = 0$

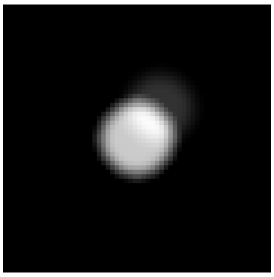
Intermediate image: $t = 0.2$

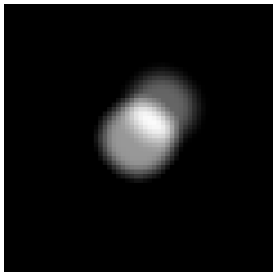
Intermediate image: $t = 0.4$

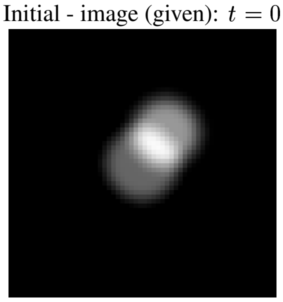
Intermediate image: $t = 0.6$

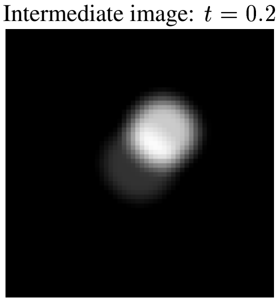
Intermediate image: $t = 0.8$

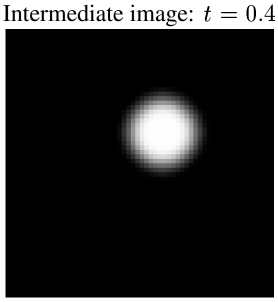
Final - image (given): $t = 1$

FIG. 4. Blending of two images with a displaced circle

Figure 5 shows an interpolating sequence between a circle and a cross; figure 6 shows an interpolating sequence between two rotated rectangles. The interpolating sequences shows the typical behavior of a fluid flow. Rigid deformations (like for instance rotations) are not captured by our interpolation model.

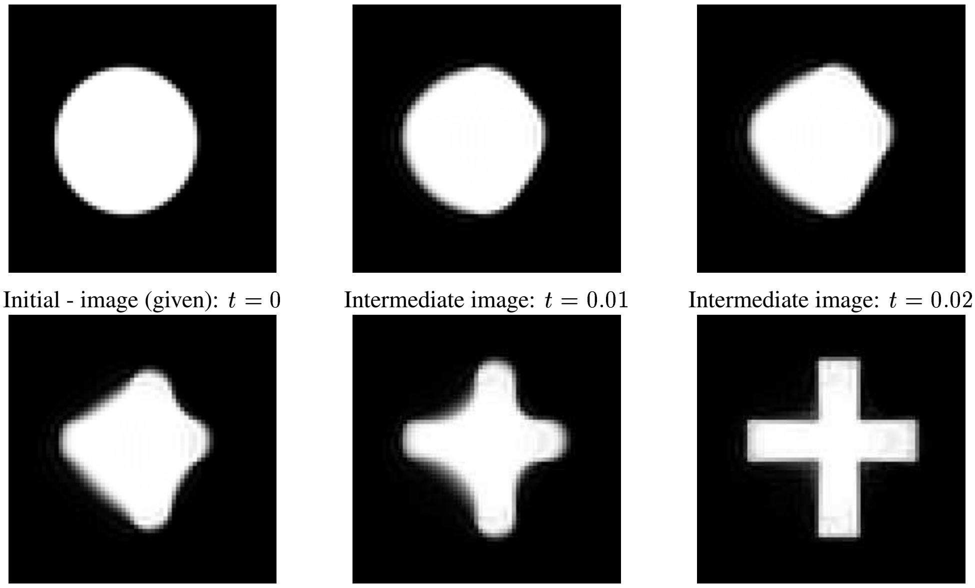

Initial - image (given): $t = 0$ | Intermediate image: $t = 0.01$ | Intermediate image: $t = 0.02$

Intermediate image: $t = 0.04$ | Intermediate image: $t = 0.08$ | Intermediate image: $t = 1$

FIG. 5. A circle becomes a cross

The finial test example shows the interpolation between MR data of brain slices of different patients. Figure 7 shows the typical behavior of our image interpolation technique. In the beginning (i.e., for small t) the global accordance is achieved. For large values of t the details are matched.

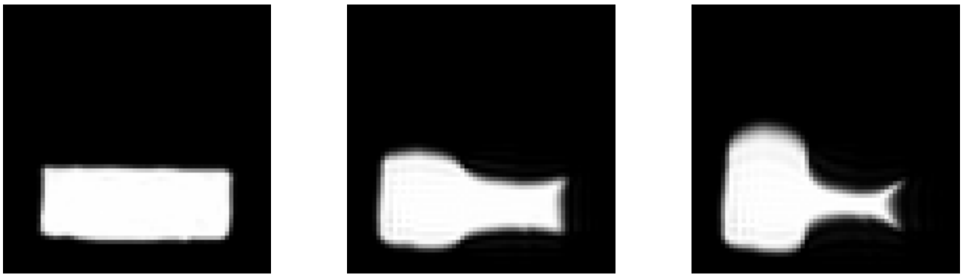

Initial - image (given): $t = 0$ Intermediate image: $t = 0.03$ Intermediate image: $t = 0.07$

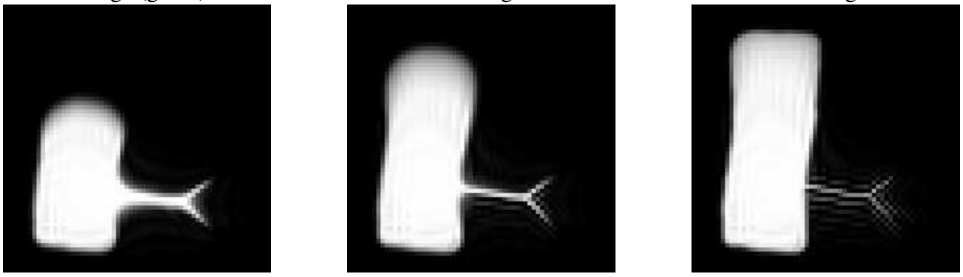

Intermediate image: $t = 0.11$ Intermediate image: $t = 0.2$ Intermediate image: $t = 1$

FIG. 6. A rectangle is rotated

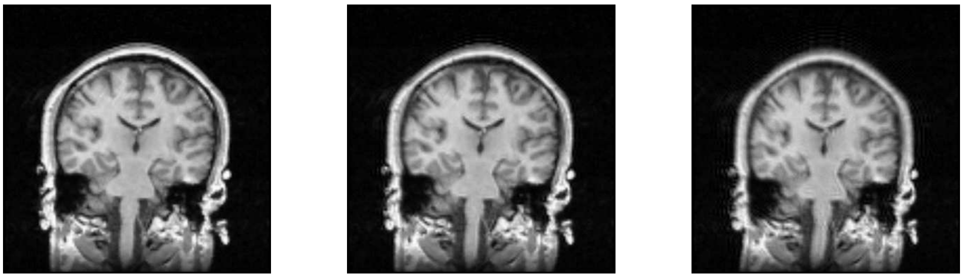

Initial - image (given) Intermediate image Intermediate image

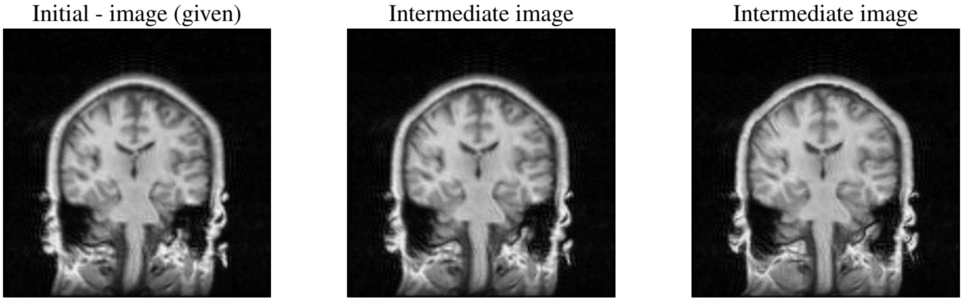

Intermediate image Intermediate image Approximation of the final image

FIG. 7. A brain gets to another brain!

ACKNOWLEDGMENT

The work of the authors is supported by the Austrian Fonds zur Förderung der wissenschaftlichen Forschung, SFB 1310. O.S. is on leave from Industrial Mathematics Institute, University of Linz.

REFERENCES

1. Aggarwal, A.; Nandhakumar, N.: *On the computation of motion from sequences of images - a review*; Proc. IEEE, 76, 917 - 935, 1988
2. Alvarez, L; Lions P.L.; Morel J.M.: *Image selective smoothing and edge detection by nonlinear diffusion II*, SIAM J. Numer. Anal. 29, 199-257, 1992.
3. Alvarez, L.; Guichard, F.; Lions, P.L.; Morel, J.M., *Axioms and fundamental equations of image processing*, Arch. Rat. Mech. Anal., 16, 200–257, 1993
4. Alvarez, L., Weickert, J., Sanchez, J.: *A scale-space approach to nonlocal optical flow calculations*, in Scale-Space Theories in Computer Vision, 235 – 246. Nielsen, M.; Johansen, P.; Olsen, O.F.; Weickert, J.; (Eds). Proceedings of the Second International Conference, Scale-Space'99, Corfu, Greece, 1999; Lecture Notes in Computer Science Vol. 1683, Springer Verlag (1999)
5. Amit, Y.; Grenander, U.; Piccioni, M.; *Structural image restoration through deformable templates*, J. Amer. Statist. Assoc. 86, 376 - 387, 1991
6. Amit, Y.; *A nonlinear variational problem for image matching*; SIAM J. Sci. Comput., 15, 207 - 224, 1994
7. Brailean, J.C.; Kleihorst R.P.; Efstratiadis, S.N.; Katsaggelos, A.K.; Lagendijk, R.L.: *Noise-reduction filters for dynamic image sequences: a review*, Proc. IEEE, 83, 1272-1292, 1995
8. Catté, F.; Lions, P.L.; Morel J.M.; Coll T.: *Image selective smoothing and edge detection by nonlinear diffusion*; SIAM J. Numer. Anal., 32, 1895 – 1909, 1992
9. Fischer, B.; Modersitzki, J.: *Fast inversion of matrices in image processing*, Numer. Algor., 22, 1 – 11, 1999
10. Horn, B.; Schunck B.: *Determining optical flow*; Artif. Intell., 17, 185 - 203, 1981
11. Lawrence E. Malvern: *Introduction to the Mechanics of a Continuous Medium*; Prentice-Hall Inc., New Jersey, 1969
12. Mitiche, A.: *Computation analysis of visual motion*, Plenum Press, New York, 1994
13. Mitiche, A.; Bouthemy, P.: *Computation and analysis of image motion: a synopsis of current problems and methods* Int. J. Comput. Vision, 19, 29–55, 1996
14. Nagel, N.H.; Enkelmann W.: *An investigation of smoothness constraints for the estimation of displacement vector fields from image sequences*, IEEE Trans. Pattern Anal. Mach. Intell., 12, 629–629, 1990
15. Nagel, N.H.: *On the estimation of optical flow: relations between new approaches and some new results*, Artif. Intell., 33, 299–324, 1987
16. Schnörr, Ch.: *Funktionalanalytische Methoden zur Gewinnung von Bewegungsinformation aus TV-Bildfolgen*, PhD Thesis, Fakultät für Informatik, University of Karlsruhe, 1991
17. Stiller, Ch.; Konrad J.: *Estimation motion in image sequences*; IEEE Signal Processing Magazine, 16, 70 - 91, 1999
18. Tekalp, A.: *Digital Video Processing*, Prentice Hall PTR, 1995
19. Weickert, J.; Schnörr Ch.: *Optic flow calculations with nonlinear smoothness terms extended into the temporal domain*, Preprint, University of Mannheim, Germany, 1999
20. Thirion, J.-P.; *Non-rigid matching using demons*, Preprint, INRIA, France
21. Weickert, J.: *On discontinuity-preserving optic flow*, Orphanoudakis, S.; Trahamnias, P.; Crowley, J.; Katveas, N.; (Eds.). Proc. Computer Vision and Mobile Robotics Workshop (CMVR'98,Santorini, 1998), 115-252, 1999
22. Weickert, J.: *Anisotropic Diffusion in Image Processing*, B. G. Teubner, Stuttgart, 1998.
23. Wloka, J.: *Partielle Differentialgleichungen*, B. G. Teubner, Stuttgart, 1982.